Hindawi
International Journal of Electrochemistry
Volume 2023, Article ID 6054452, 9 pages
https://doi.org/10.1155/2023/6054452

Research Article

Enabling the Electrochemical Performance of Maricite-$NaMnPO_4$ and Maricite-$NaFePO_4$ Cathode Materials in Sodium-Ion Batteries

Ijaz Ul Mohsin[1], **Luca Schneider**[2], **Zheng Yu**[1], **Wenqing Cai**[1], and **Carlos Ziebert**[1]

[1]*Institute of Applied Materials, Applied Materials Physics (IAM-AWP), Karlsruhe Institute of Technology, Karlsruhe, Germany*
[2]*Institute of Applied Materials, Energy Storage System (IAM-ESS), Karlsruhe Institute of Technology, Karlsruhe, Germany*

Correspondence should be addressed to Ijaz Ul Mohsin; ijaz.mohsin@kit.edu

Received 26 October 2022; Revised 18 January 2023; Accepted 18 January 2023; Published 27 January 2023

Academic Editor: Arulraj Arunachalam

$NaMnPO_4$ and $NaFePO_4$, polyanion cathode materials, exist in two different phases maricite/natrophilite and maricite/olivine, respectively. Both natrophilite $NaMnPO_4$ and olivine $NaFePO_4$ are electrochemically active and possess a one-dimensional tunnel for sodium-ion migration; however, these two phases are thermodynamically unstable. Therefore, they can be synthesized through an electrochemical route. On the contrary, maricite (m)-$NaMnPO_4$ and maricite (m)-$NaFePO_4$ are thermodynamically stable forms but have a huge activation energy of their diffusion pathways for sodium extraction and insertion in the crystal structure, which hinders electrochemical reactions. Therefore, the electrochemical behaviour of commercial m-$NaMnPO_4$ and m-$NaFePO_4$ has been studied to find a way for enabling them electrochemically. Ball milling and thermal/mechanical carbon coating are employed to reduce the particle size to enhance the electrochemical performance and shorten the diffusion pathway. Moreover, ball milling leads to defects and partial phase transformation. The electrochemical performance of milled-coated $NaMnPO_4$ and $NaFePO_4$ has been thoroughly investigated and compared. The phase transition of $NaFePO_4$ is revealed by a differential scanning calorimeter. As a result, the achievable capacities of both cathode materials are significantly enhanced up to ~50 mAh.g^{-1} via the particle size reduction as well as by carbon coating. However, the side reactions and agglomeration problems in such materials need to be minimized and must be considered to enable them for applications.

1. Introduction

In the past few years, sodium-ion batteries (SIBs) appear as an alternative due to their low cost and abundance of the raw materials, which make SIBs extremely suitable for large-scale stationary applications [1, 2] by having a similar working mechanism as known from lithium-ion batteries [3]. Despite the advantages, the redox potential and ionic radius of sodium ions make intercalation/deintercalation more difficult than for lithium ions [4, 5]. These factors result in lower energy density, lower electrochemical stability, and shorter battery life. Among the transition metals, Fe and Mn are mostly used as the transition metal element for the polyanions because of their environmental friendliness and their low costs [6]. In the olivine structure of $NaFePO_4$, there are three possible ways for the sodium ion migration and migration energies of sodium ions along different paths are shown in literature [7] and only a 1D channel for the sodium ion migration exists, which makes $NaFePO_4$ intrinsically low ionic conductive. In comparison with Schottky and Frenkel defects, the formation of antisite defects [8] is much more energy-efficient, which means the antisite defects are more favorable for migration. One method to improve the electrochemical properties is to reduce the particle size, which reduces the diffusion path length and increases the contact area with the carbon black. Drezen et al. [6] have systematically studied the effect of the particle size on the olivine structure for $LiMnPO_4$. However, Kim et al. [9] reported an unexpected finding in maricite $NaFePO_4$ in 2015. According to their study, maricite $NaFePO_4$ exhibits more than 90% of its theoretical capacity and outstanding cyclability. Various polyanion cathode materials for SIBs have been reported, such as $NaFePO_4$, Na_2FePO_4F, $Na_2FeP_2O_7$, and $Na_4Fe(PO_4)_2P_2O_7$

[10–12]. However, $NaMnPO_4$ is seldom reported as the active material for battery application, due to its low achievable capacity. Nevertheless [13], the theoretical capacity of $NaMnPO_4$ and its crystal structure is similar to $NaFePO_4$ (154 mAh.g^{-1}) [14]; therefore, it is still worth investigating $NaMnPO_4$ and $NaFePO_4$ materials.

The focus of this work is to enable m-$NaMnPO_4$ and m-NaFePO4 cathode materials and improve their electrochemical properties by means of reducing particle size accompanied by carbon coating as reported in the literature [15, 16] for other cathode materials. Therefore, m-$NaMnPO_4$ and m-NaFePO4 powders were milled to fine particle sizes followed by carbon coating by utilizing different carbon sources using a thermal/mechanical approach to enhance the electrochemical performance.

2. Experimental Methods

In order to determine the elemental composition of the active cathode materials, the ICP- OES (OPTIMA 4300 DV Perkin Elmer) technique was used, and the oxygen content was analyzed with the method of carrier gas hot extraction (CGHE) by the oxygen/nitrogen analyzer TC600 (LECO).

The laser scattering (Horiba Partica LA-950) method was used to determine the particle size distribution of commercial m-$NaMnPO_4$ and m-$NaFePO_4$ powder materials from the NEI corporation.

These materials were also studied by powder X-ray diffraction through a SEIFERT X-ray diffractometer, and Cu Kα ($\lambda = 1.54056$ Å) was used as the X-ray source. The powder materials were fixed on the ω-axis. The scanning angle was from 10° to 70°, with a step size increment of 0.01°.

The m-$NaMnPO_4$ and m-$NaFePO_4$ powder materials were reduced to smaller particle sizes by a ball mill (Pulverisette 7 premium, Fritsch) at 1000–1200 rpm for 12 h with an interval of 30 min with a rest time of 2 h. To minimize the contamination during the ball milling process, a nylon jar and high purity yttrium stabilized ZrO_2 balls (1 mm diameter) were used to grind the pristine m-$NaMnPO_4$ and m-$NaFePO_4$ (active material : balls = 1 : 80 by weight). In this work, the wet (isopropanol) grinding method was chosen to achieve a better grinding effect. On the one hand, the liquid can reduce the surface tension of small particles, especially nanoparticles, and on the other hand, the liquid can slow down the temperature rise and provide safety. The ground materials were subsequently vacuum-dried (10^{-3} bar) at 70°C for 12 h. Glucose (10 wt.%) was dissolved in distilled water, and then, active material m-$NaFePO_4$ was added to this solution and further mixed uniformly with a speed mixer (DC 150) followed by calcination at 600°C under an Ar atmosphere.

To coat the active material milled $NaMnPO_4$ with carbon black, a mechanochemical process was employed. At first, the carbon black (20 wt.%) was mixed with active material 2 : 8 by weight and milled for 3 hours at 1200 rpm with an interval of 30 min accompanied by drying at 400°C with a holding time of 4 hours. Finally, the carbon-coated m-$NaMnPO_4$ and m-$NaFePO_4$ materials were analyzed by scanning electron microscopy (SEM) (Supra 55, Zeiss) to confirm that the coating process was successful.

Since it was necessary to coat the cathode materials with carbon up to a certain temperature under Ar atmosphere, the determination of the phase transformation during the heating of the pristine materials was essential. A differential scanning calorimeter (NETZSCH DSC 404) was utilized in this investigation using an Al_2O_3 crucible under an Ar gas flow of 100 ml/min. In the case of $NaFePO_4$, a heating rate of 5 K/min temperature was used from room temperature to 600°C, and for $NaMnPO_4$, the heating rate of 10 K/min was applied up to 900°C.

A NETZSCH TG 449 F1 Jupiter thermal nanobalance coupled with the NETZSCH QMS 403C mass spectrometer (MS) was used to investigate the thermal stability of the cathode materials with respect to the phase transformation as indicated in the differential scanning calorimeter (DSC) measurement. The fused silica transfer lines (75 μm diameter) leading to the MS were heated to 200°C to ensure that all the samples entered the MS in a gaseous state, i.e., to avoid condensation losses. An alumina sample holder was used for the measurements.

The respective slurries were prepared by dissolving 10 wt.%. polyvinylidene fluoride (PVDF) binder in a N-methyl-2-pyrrolidone (NMP) organic solvent using 80 wt.% active cathode materials (including carbon coating) and 10 wt.% carbon black (C-NERGY Super C65). The slurries were coated on an Al foil (19 μm) and were dried at 70°C for 1 day under vacuum (10^{-3} bar). Dried cathode sheets were calendered by 10–15% using a calendering machine (Hot Rolling Press with Variable Speed, MTI) followed by subsequent drying at 120°C under vacuum (10^{-3} bar) for 1 day. Calendered sheets were punched into 13 mm diameter discs. In order to study the electrochemical properties of pristine and milled carbon-coated m-$NaMnPO_4$ and m-$NaFePO_4$ materials, coin cells (CR-2032) were assembled against pure Na metal as the anode material with 1 M $NaClO_4$ (EC : DMC 1 : 1 vol % + 5 vol % FEC) electrolyte of 100 μl and glass fiber separator (GF/A from Whatman) in an Ar-filled glovebox ($H_2O < 0.1$ ppm, $O_2 < 0.1$ ppm). The electrochemical data were recorded with a BioLogic instrument (MPG2). The coin cells were charged and discharged at a C/10 rate during a constant current (CC) phase in the voltage range of 1.0–4.5 V (m-$NaMnPO_4$) and 1.5–4.5 V (m-$NaFePO_4$).

3. Results and Discussion

With respect to the elemental analysis results, the stoichiometric ratios of Na, Mn, Fe, P, and O are shown in Table 1, and commercial cathode materials (pristine) stoichiometry is confirmed as m-$NaMnPO_4$ and m-$NaFePO_4$.

Thermal carbon coating of m-$NaFePO_4$ is performed under an argon atmosphere. However, it is observed that the color of the sample powder changes after 12 h of milling before and after calcination, i.e., a chemical reaction occurred during the high-temperature heating process of the sample in the argon atmosphere. In addition, the calcination process further increases the oxygen content, and the stoichiometric ratio of oxygen content increases to 4.57 (compared to the milled m-$NaFePO_4$ powder oxygen content of 4.29). It is suggested that oxidation occurs during the

Table 1: Elemental stoichiometry of pristine m-$NaMnPO_4$ and m-$NaFePO_4$ powders.

	Elements	Na	Fe	Mn	P	O
m-$NaMnPO_4$	Mass fraction	12.80 (±0.2)	—	30.80 (±0.2)	18.20 (±0.2)	36.80 (±0.4)
	Stoichiometric ratio	1.0	—	1.01	1.05	4.13
m-$NaFePO_4$	Mass fraction	13.36 (±0.06)	30.90 (±0.1)	—	17.30 (±0.1)	35.50 (±0.3)
	Stoichiometric ratio	1.0	0.95	—	0.97	3.83

high-temperature heat treatment, as the carbon source (glucose) is dissolved in water to have a homogenous mixture before calcination. Such an increase in oxygen content occurs and relates to the oxidation of iron (II) to iron (III) beyond 520°C. By comparison with the XRD diffractogram, it is evident that calcination causes recrystallization and the newly formed crystals contain a presumably olivine/oxidized-$NaFePO_4$@C structure (see Figure 1). Therefore, by means of elemental chemical analysis, the substances before and after calcination are measured again to verify the composition of the product.

3.1. $NaMnPO_4$ Material. The morphology of pristine m-$NaMnPO_4$ is made up of rod-like aggregates and the particle size is from several micrometers to one hundred micrometers, which makes the pristine m-$NaMnPO_4$ not suitable for battery applications. Figure 2 shows the particle size distribution of pristine m-$NaMnPO_4$ (Figure 2(A)) and milled $NaMnPO_4$ ($d_{50} = 400$ nm) (Figure 2(C)) in accordance with SEM images, respectively, in Figures 2(B) and (D) (milled + coated/covered with carbon). The particle size of $NaMnPO_4$ is reduced to $d_{50} = 400$ nm during ball milling and the result shows the bimodal distribution, indicating (Figure 2(C)) that any further extension of the milling time has little impact on the particle size. Additionally, Figure 2(D) shows the SEM images of milled $NaMnPO_4$@C partially covered carbon particles and the change in the morphology of particles into a sponge-like structure. It is most probable that the sponge-like structure is due to the C coating. At the same time, it can also be seen that ball milling with 1 mm ZrO_2 grinding beads cannot reduce the particle size to the level of 50–100 nm, which is the required size reported in the literature [17]. The different grinding balls (2 mm and 1 mm) were used to reduce the particle size, and particle distribution is shown in the supplementary material (see Figure S1). With smaller grinding balls of 1 mm ZrO_2, the 400 nm (d_{50}) particles were achieved.

All peaks that are observed in the XRD pattern of the pristine m-$NaMnPO_4$ (see Figure 3)match with the maricite structure as reported for m-$NaMnPO_4$ [18]. After milling and carbon covering, the intensity of the XRD peaks increases and indicates improved crystallization and crystallite growth. Theoretically, the m-$NaMnPO_4$ could transfer into natrophilite $NaMnPO_4$ and amorphous $NaMnPO_4$ [9]. Therefore, the newly formed peaks are compared with the standard natrophilite NaMnPO4 XRD pattern and are found to be in accordance with it. These peaks are highlighted by the red line. These peaks clearly demonstrate the increase of the natrophilite $NaMnPO_4$ content [9]. The SEM image of milled 40 nm $NaMnPO_4$ without carbon coating for better comparison is listed in the supplementary material (see Figure S2).

In Figure 4, the thermal analysis of m-$NaMnPO_4$ is presented. According to this result, two endothermic peaks during the heating and one exothermic peak during the cooling steps are observed. The occurrence of the first endothermic peak is due to the decomposition/transformation of m-$NaMnPO_4$ into new phases as impurity [19]. The second endothermic peak shows that m-$NaMnPO_4$ melts at 839.7°C, which is reversible, and an exothermic peak is clearly observed during the cooling phase at 810°C (crystallization/solidification). According to the result, there is no change in the material up to 700°C, which demonstrates that there is no phase transition/decomposition. Hence, the thermal procedure with carbon black at 400°C is a safe choice. Furthermore, the TGA-MS result of m-$NaMnPO_4$ (see Figure S3 (Supplementary Material)) shows material thermal stability up to 900°C (at 727°C, it is nonvolatile).

In Figure 5, the comparison of the achievable capacities of m-$NaMnPO_4$ with pristine and fine carbon-coated particles is shown. For $NaMnPO_4$@C, the maximum capacity is 47 $mAh.g^{-1}$ in the third cycle, which is significantly higher than that of the pristine material. This indicates that particle size and carbon coating play an important role in enhancing capacity. The cyclability of pristine and milled/coated at different particle sizes is shown in the supplementary material (see Figure S4) and a comparison was made. However, it is worth mentioning that the achievable capacity of $NaMnPO_4$@C (400 nm) could be expected to be even higher. A reasonable explanation for not having a higher specific capacity of this fine partially coated/covered material could be that the nanoparticles exhibit high surface energy and tend to form agglomerations. However, the shear force of the speed mixer is not strong enough to break these agglomerations. Therefore, the active material could not be dispersed homogeneously in the slurry. EDX analysis in supplementary Figure S7 confirms the elemental distribution of $NaMnPO_4$ with carbon contents. During charging, the Mn^{2+} intercalates with the sodium atoms and Mn^{2+} oxidizes to Mn^{3+}, and upon discharge, the sodium intercalates, reducing Mn^{3+} to Mn^{2+}.

3.2. $NaFePO_4$ Material. In Figure 6, the particle size distribution and SEM images of the pristine (Figure 6(A)/(B)), 12 h milled (Figure 6(C)/(D)), and milled-coated $NaFePO_4$ (Figure 6(E)/(F)) are shown. During ball milling, the particle size is reduced to $d_{50} = 1.57\,\mu$m and is evenly distributed. By coating with glucose and after calcination, it is observed that the particle size becomes larger (about $d_{50} = 3.5\,\mu$m). This is because of agglomeration during the mixing of active

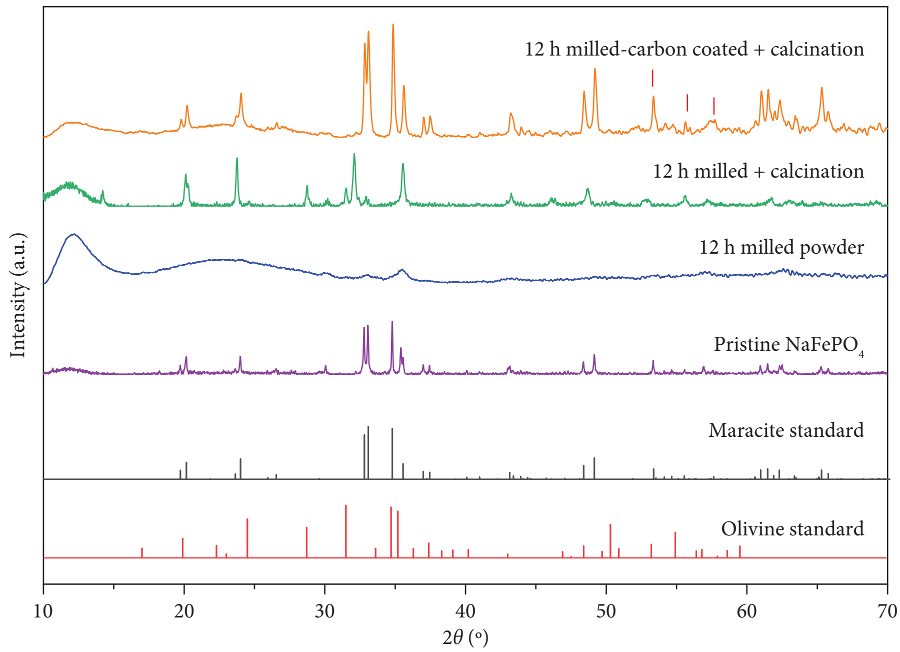

Figure 1: XRD pattern of 12 h ground m-$NaFePO_4$ (before/after calcination) compared to the pristine material.

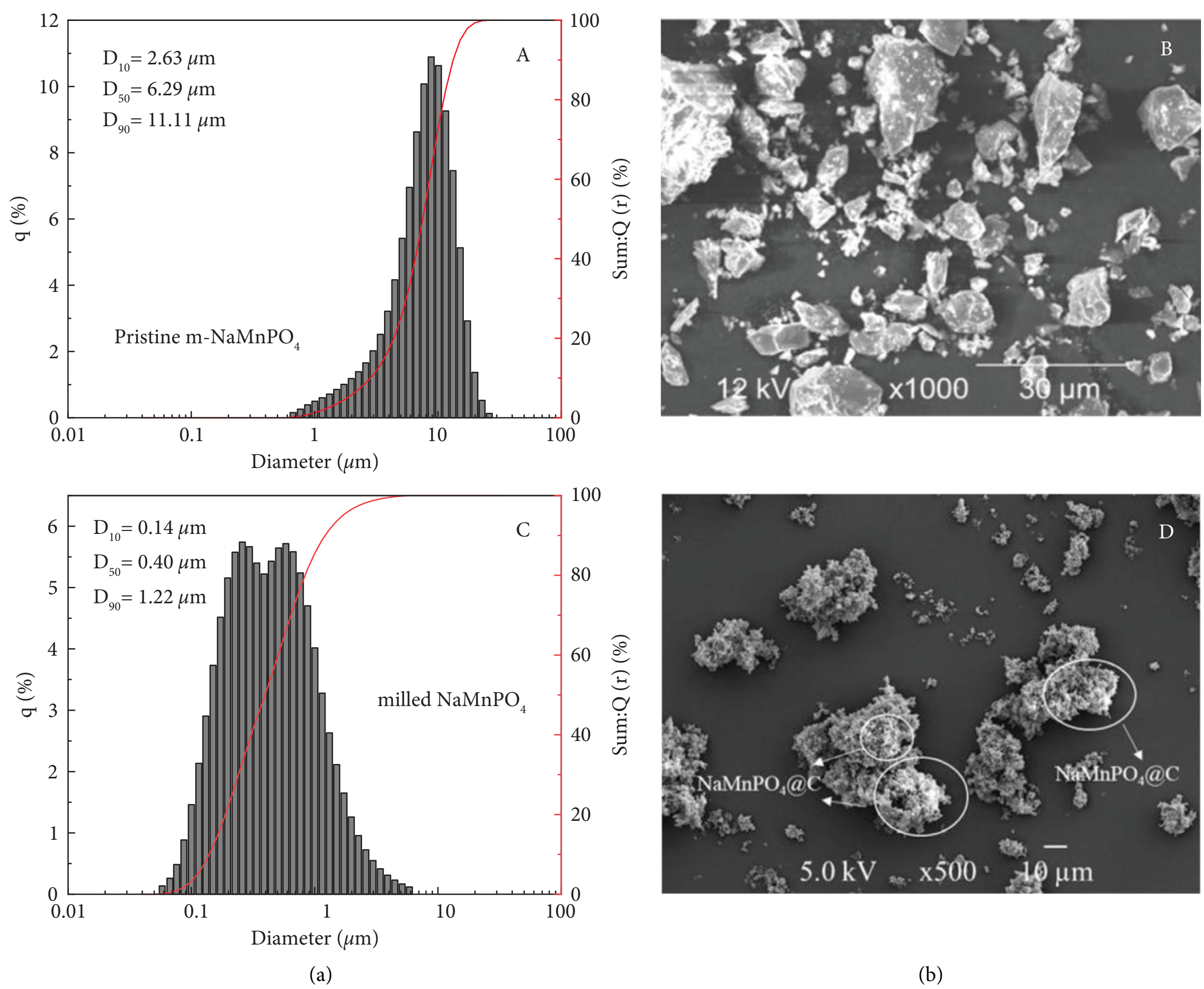

Figure 2: Particle size distribution (a) and SEM images (b) of $NaMnPO_4$ powder: (A) and (B) pristine, (C) and (D) 12 h-coated milled $NaMnPO_4$.

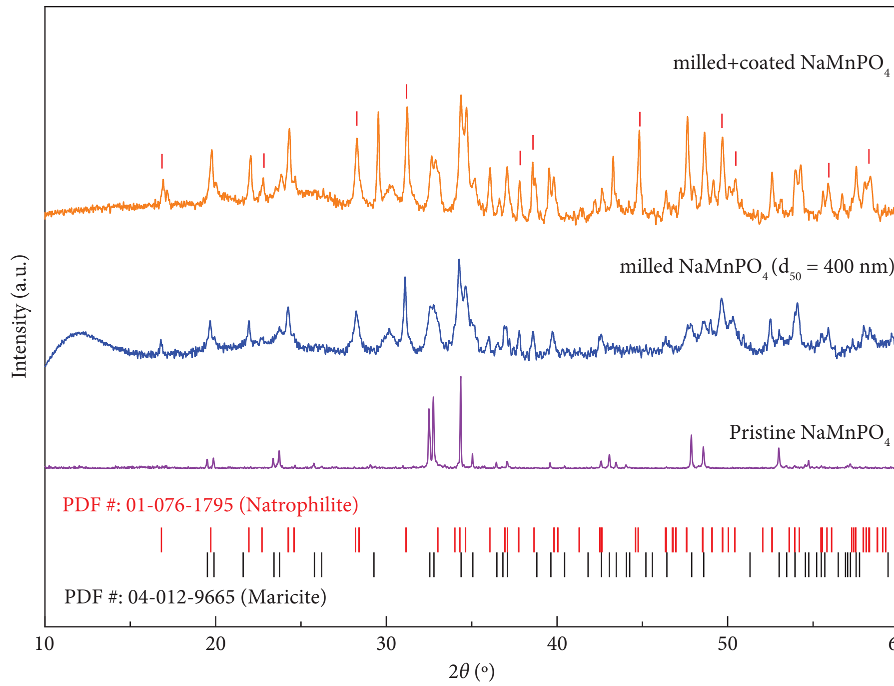

Figure 3: The XRD patterns of pristine m-$NaMnPO_4$ and milled/milled-coated $NaMnPO_4$ (400 nm).

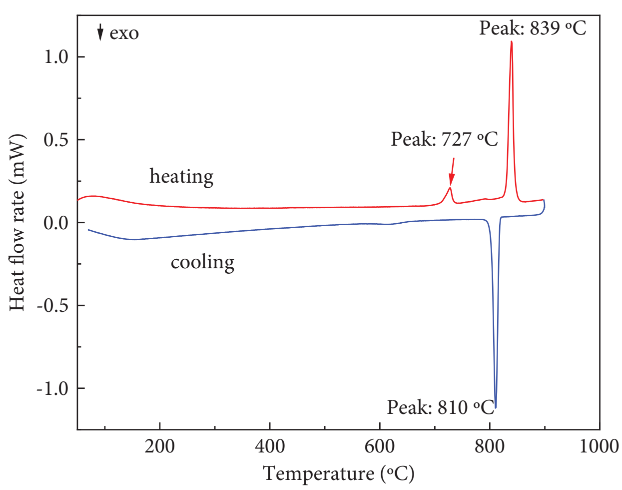

Figure 4: DSC diagram of pristine m-$NaMnPO_4$.

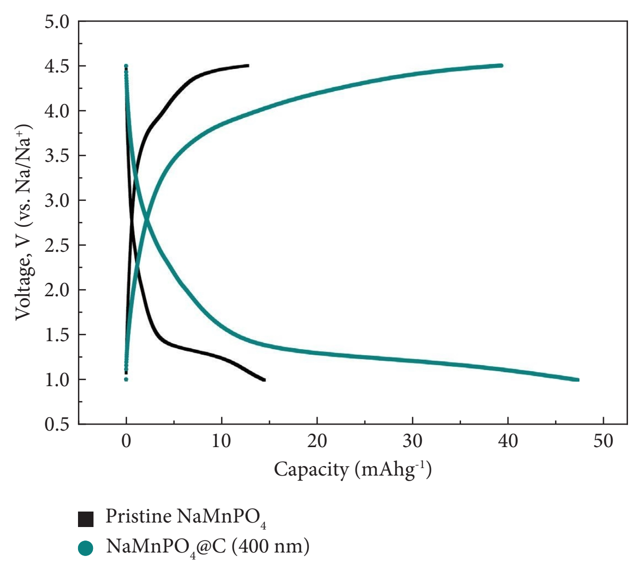

Figure 5: Electrochemical performance of pristine and milled-coated $NaMnPO_4$ (cycle number 3).

material with glucose solution (water as a solvent), as seen in the SEM image as well (see Figures 6(f), S5 at higher magnification (Supplementary Materials)).

In the diffractogram of pristine m-$NaFePO_4$, shown in Figure 1, all the reflections are in agreement with the maricite structure from JCPDS file #04-012-9665 [20]. After grinding and dissolution in a glucose solution, the m-$NaFePO_4$ powder is calcined and recrystallized. It is obvious that new reflections appear (highlighted in red). These reflections can be partially assigned to the olivine structure. It can be assumed that calcination up to 600°C causes a phase transformation from m-$NaFePO_4$ to olivine $NaFePO_4$, which can be observed in DSC thermal analysis as well, as discussed later in the article. To verify whether the ball milling process causes amorphization or the subsequent high-temperature heat treatment causes recrystallization, additional comparative tests are performed. The 12 h ground powder was taken out and heat-treated separately (without glucose), i.e., without carbon coating. It is found that the results are consistent with those in the carbon-coated condition, and this finding is also consistent with the results reported by Hwang et al. [14]. They indicated that ball-milled m-$NaFePO_4$ partly contains an amorphous phase and longer ball-milling (24 h) did not result in complete amorphization. Therefore, it is concluded that high-temperature heat treatment up to 600°C can recrystallize the amorphous $NaFePO_4$.

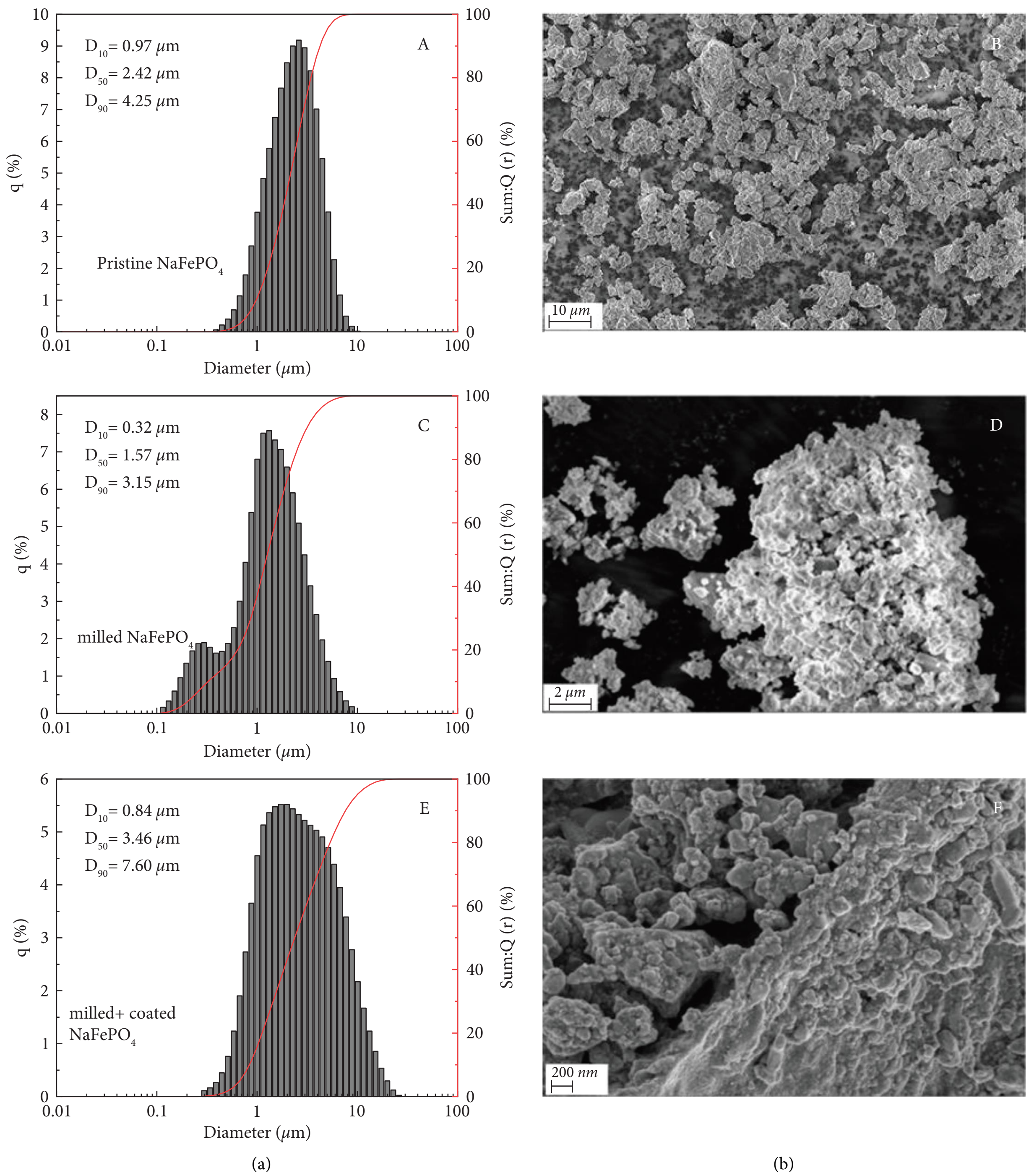

Figure 6: Particle size distribution (a) and SEM images (b) of $NaFePO_4$ powder: (A) and (B) pristine, (C) and (D) milled, (E) and (F) milled-glucose coated (calcinated).

Afterward, the possible phase changes between room temperature and 600°C were investigated, because the coating is thermally processed at 600°C under an argon atmosphere. No phase change was found in pristine m-$NaFePO_4$ (Figure 7). Surprisingly, a large exothermic peak is observed at 390°C in the case of milled m-$NaFePO_4$ (without calcination), which means that the ball-milled powder undergoes a significant phase change at 390°C. The newly formed phase is presumably olivine $NaFePO_4$/oxidized-$NaFePO_4$ phases, and subsequently, carbon coating is made by the method used for $LiFePO_4$ [21]. After the temperature treatment at 600°C, the milled powder partly changed its color from black to orange. Comparing the X-ray diffractograms in Figure 1, it can be concluded that the ball milling process amorphized m-$NaFePO_4$, and then, the calcination process recrystallized it, but the crystal structure is no longer pure maricite afterward. On the one hand, this newly formed substance could be oxidized-

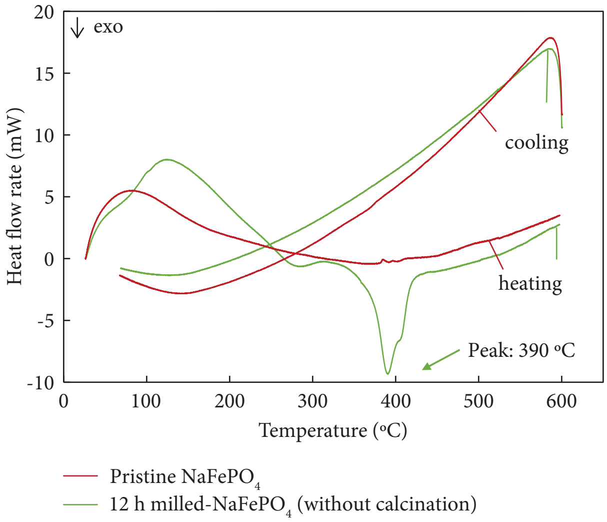

Figure 7: DSC diagram of 12 h ground (uncalcined) m-$NaFePO_4$ (green) compared to that of original $NaFePO_4$ (red).

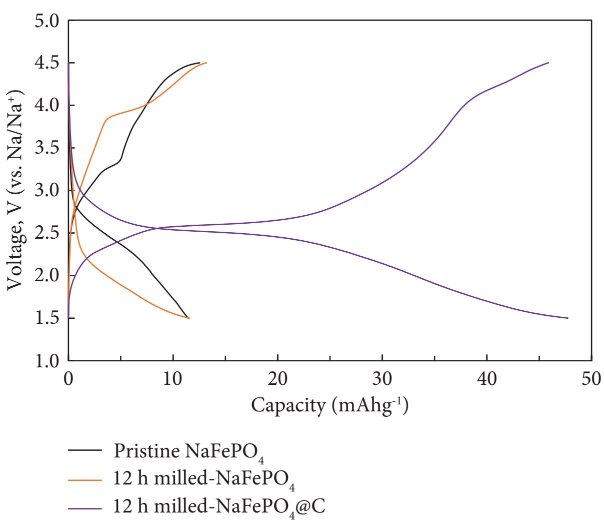

Figure 8: Comparison of electrochemical performance of pristine, milled, and milled-coated $NaFePO_4$ materials (cycle number 3).

$NaFePO_4/FePO_4$ (as oxygen content increased, see Table 1), as transforming the maricite phase into electrochemically active amorphous $FePO_4$ is reported in literature [22, 23] and this phase exhibits a reversible capacity of 142 mAh.g^{-1} at room temperature [9]; on the other hand, it could consist of a mixture of olivine $NaFePO_4$ and impurity compounds with Na, Fe, P, O (such as Xenophyllite $Na_4Fe_7(PO_4)_6$, or NASICON-type $Na_3Fe_2(PO_4)_3$) [24]. Regarding the phase change of milled m-NaFePO4 at 390°C, unfortunately, no information is reported in the literature. Therefore, this needs to be further investigated in future studies. Subsequently, no noticeable material loss/outgassing (nonvolatile transformation) is observed until 600°C (see Figure S6, supplementary material). EDX analysis in supplementary Figure S8 confirms the elemental distribution of $NaFePO_4$ with carbon contents.

Figure 8 shows the galvanostatic measurement results on coin cells made with pristine m-$NaFePO_4$, 12 h milled (amorphous phase not calcinated), and 12 h milled + calcinated at 600°C (mixed with glucose) active cathode materials. A capacity of nearly 48 mAh.g^{-1} is achieved in the case of milled-coated material. Nevertheless, 12 h milled powder without calcination shows no change in electrochemical performance. This result confirms the hypothesis of Ellis et al. [25] in part and the result of Zaghib et al. [26] regarding the difficulty to remove sodium from maricite materials. This underlines that extended grinding transforms the material into an amorphous phase, which is consistent with the XRD analysis (Figure 1). It is interesting to note that a distinct plateau region is observed in the charge and discharge curves at 2.6 V, which is also reported for Li_2MnSiO_4@C (glucose as a source for carbon) cathode by Devaraj et al. [27] and recently by Boyadzhieva et al. for m-$NaFePO_4$ [28]. The appearance of this plateau indicates the characteristics of the phase transformation in the crystal structure [29]. This plateau expresses an increase of capacity of around 25 mAh.g^{-1} (50% of achieved capacity). This result further proves that 12 h ground $NaFePO_4$ with the calcination (with coating) process produces partly a mixture of olivine structure/oxidized-$NaFePO_4$@C, which is comparable to electrochemical data in reference [13]. The maricite $NaMnPO_4$ is in the Fe^{2+} oxidation state, in which the sodium intercalates during charging and Fe^{2+} oxidizes to the Fe^{3+} state. While discharging, the sodium deintercalates and reduces from Fe^{3+} to Fe^{2+} oxidation state.

4. Conclusions

To enable and improve the electrochemical performance of the maricite electrode materials, milling and carbon coating were implemented and the electrochemical performance of the respective half-coin cells was investigated and compared. The pristine m-$NaMnPO_4$ and m-$NaFePO_4$ showed a very low achievable capacity (electrochemically inactive) and milling combined with carbon coating facilitates the electron transport, which demonstrates better cell performances with discharge capacities of ~50 mAh.g^{-1} in both materials. However, the long milling time (12 h) caused m-NaFePO4 to undergo an amorphous phase change, yielding no significant change in the capacity without calcination instead. This study also suggests that many other inactive materials can be converted into active materials by a combination of nanosizing and carbon coating procedures. The nanosized particles reduce the diffusion pathway in process of intercalation and increase the active surface area, which facilitates enhancement of the electrochemical performance. However, due to poor electronic conductivity, additives like carbon or fluorine are used to increase the electronic conductivity.

Data Availability

The data used to support the findings of this study are available from the corresponding author on reasonable request.

Conflicts of Interest

The authors declare that they have no conflicts of interest.

Acknowledgments

The authors gratefully acknowledge the support of Dr. T. Bergfeldt for elemental analysis (ICP-OES) and Dr. K. Seemann for XRD analysis. This work contributes to the research performed at CELEST (Center for Electrochemical Energy Storage Ulm-Karlsruhe). This work was funded by the German Research Foundation (DFG) under Project ID 390874152 (POLiS Cluster of Excellence).

Supplementary Materials

Figure S1: Milled NaMnPO4; (a) milled with 2 mm ZrO_2 balls and (b) milled with 1 mm ZrO_2 ball; Figure S2: SEM image of milled $NaMnPO_4$ (400 nm) without carbon coating at different magnifications; Figure S3: Thermogravimetric plot of m-$NaMnPO_4$ with evolved gases; Figure S4: cyclability cycles of $NaMnPO_4$; (a) Pristine, (b) 2.12 μm milled coated, (c) 1.15 μm milled coated, and (d) 400 nm milled coated; Figure S5: SEM image of milled-glucose coated $NaFePO_4$; Figure S6: Thermogravimetric plot of m-$NaFePO_4$ with evolved gases; Figure S7: EDX element distribution of $NaMnPO_4$@C; Figure S8: EDX element distribution of $NaFePO_4$@C with glucose coating. (*Supplementary Materials*)

References

[1] J. Y. Hwang, S. T. Myung, and Y. K. Sun, "Sodium-ion batteries: present and future," *Chemical Society Reviews*, vol. 46, no. 12, pp. 3529–3614, 2017.
[2] S. M. Oh, S. W. Oh, C. S. Yoon, B. Scrosati, K. Amine, and Y. K. Sun, "High-performance carbon-$LiMnPO_4$ nanocomposite cathode for lithium batteries," *Advanced Functional Materials*, vol. 20, no. 19, pp. 3260–3265, 2010.
[3] J. Zhao, L. Zhao, K. Chihara et al., "Electrochemical and thermal properties of hard carbon-type anodes for Na-ion batteries," *Journal of Power Sources*, vol. 244, pp. 752–757, 2013.
[4] M. S. Islam and C. A. J. Fisher, "Lithium and sodium battery cathode materials: computational insights into voltage, diffusion and nanostructural properties," *Chemical Society Reviews*, vol. 43, no. 1, pp. 185–204, 2014.
[5] G. Wang, F. Wang, P. Zhang et al., "Polarity-switchable symmetric graphite batteries with high energy and high power densities," *Advanced Materials*, vol. 30, no. 39, Article ID 1802949, 2018.
[6] T. Drezen, N.-H. Kwon, P. Bowen, I. Teerlinck, M. Isono, and I. Exnar, "Effect of particle size on $LiMnPO_4$ cathodes," *Journal of Power Sources*, vol. 174, no. 2, pp. 949–953, 2007.
[7] R. Tripathi, S. M. Wood, M. S. Islam, and L. F. Nazar, "Na-ion mobility in layered Na_2FePO_4F and olivine Na[Fe,Mn]PO4," *Energy and Environmental Science*, vol. 6, no. 8, pp. 2257–2264, 2013.
[8] J. C. Phillips, "Semiconductor compounds and alloys," *Electronic States of, Encyclopedia of Condensed Matter Physics*, vol. 5, pp. 256–264, 2005.
[9] J. Kim, D.-H. Seo, H. Kim et al., "Unexpected discovery of low-cost maricite $NaFePO_4$ as a high-performance electrode for Na-ion batteries," *Energy and Environmental Science*, vol. 8, no. 2, pp. 540–545, 2015.
[10] C.-Y. Chen, K. Matsumoto, T. Nohira, R. Hagiwara, Y. Orikasa, and Y. Uchimoto, "Pyrophosphate Na2FeP2O7 as a low-cost and high-performance positive electrode material for sodium secondary batteries utilizing an inorganic ionic liquid," *Journal of Power Sources*, vol. 246, pp. 783–787, 2014.
[11] Y. Zhu, Y. Xu, Y. Liu, C. Luo, and C. Wang, "Comparison of electrochemical performances of olivine NaFePO4 in sodium-ion batteries and olivine LiFePO4 in lithium-ion batteries," *Nanoscale*, vol. 5, no. 2, pp. 780–787, 2013.
[12] P. Barpanda, T. Ye, S. i. Nishimura et al., "Sodium iron pyrophosphate: a novel 3.0 V iron-based cathode for sodium-ion batteries," *Electrochemistry Communications*, vol. 24, pp. 116–119, 2012.
[13] V. Priyanka, G. Savithiri, R. Subadevi, and M. Sivakumar, "An emerging electrochemically active maricite NaMnPO4 as cathode material at elevated temperature for sodium-ion batteries," *Applied Nanoscience*, vol. 10, pp. 3945–3951, 2020.
[14] J. Hwang, K. Matsumoto, Y. Orikasa et al., "Crystalline maricite NaFePO4 as a positive electrode material for sodium secondary batteries operating at intermediate temperature," *Journal of Power Sources*, vol. 377, pp. 80–86, 2018.
[15] G. T. K. Fey, Y. G. Chen, and H.-M. Kao, "Electrochemical properties of $LiFePO_4$ prepared via ball-milling," *Journal of Power Sources*, vol. 189, no. 1, pp. 169–178, 2009.
[16] Y. Liu, N. Zhang, F. Wang, X. Liu, L. Jiao, and L.-Z. Fan, "Approaching the downsizing limit of maricite NaFePO4 toward high-performance cathode for sodium-ion batteries," *Advanced Functional Materials*, vol. 28, no. 30, Article ID 1801917, 2018.
[17] T. Boyadzhieva, V. Koleva, E. Zhecheva, D. Nihtianova, L. Mihaylov, and R. Stoyanova, "Competitive lithium and sodium intercalation into sodium manganese phospho-olivine $NaMnPO_4$ covered with carbon black," *RSC Advances*, vol. 5, no. 106, pp. 87694–87705, 2015.
[18] P. T. Kissinger and W. R. Heineman, "Cyclic voltammetry," *Journal of Chemical Education*, vol. 60, no. 9, p. 702, 1983.
[19] I. V. Korchemkin, I. V. Pet'kov, V. S. Kurazhkovskaya, and E. Yu. Borovikova, "Synthesis of sodium nickel phosphate and its crystallographic, spectroscopic, and temperature-controlled X-ray diffraction study," *Russian Journal of Inorganic Chemistry*, vol. 60, no. 3, pp. 265–269, 2015.
[20] M. D. Slater, D. Kim, E. Lee, and C. S. Johnson, "Sodium-ion batteries," *Advanced Functional Materials*, vol. 23, no. 8, pp. 947–958, 2013.
[21] Y. Zhu and C. S. Wang, "Galvanostatic intermittent titration technique for phase-transformation electrodes," *Journal of Physical Chemistry C*, vol. 114, no. 6, pp. 2830–2841, 2010.
[22] Y. J. Yin, Y. J. Hu, P. Wu, H. Zhang, and C. X. Cai, "A graphene–amorphous FePO4 hollow nanosphere hybrid as a cathode material for lithium ion batteries," *Chemical Communications*, vol. 48, no. 15, pp. 2137–2139, 2012.
[23] Y. J. Lee and A. M. Belcher, "Nanostructure design of amorphous FePO4 facilitated by a virus for 3 V lithium ion battery cathodes," *Journal of Materials Chemistry*, vol. 21, no. 4, pp. 1033–1039, 2011.
[24] P. P. Prosini, C. Cento, A. Masci, and M. Carewska, "Sodium extraction from sodium iron phosphate with a Maricite structure," *Solid State Ionics*, vol. 263, pp. 1–8, 2014.
[25] B. L. Ellis, W. R. M. Makahnouk, W. N. Rowan-Weetaluktuk, D. H. Ryan, and L. F. Nazar, "Crystal structure and

electrochemical properties of A2MPO4F fluorophosphates (A = Na, Li; M = Fe, Mn, Co, Ni)," *Chemistry of Materials*, vol. 22, no. 3, pp. 1059–1070, 2009.

[26] K. Zaghib, J. Trottier, P. Hovington et al., "Characterization of Na-based phosphate as electrode materials for electrochemical cells," *Journal of Power Sources*, vol. 196, no. 22, pp. 9612–9617, 2011.

[27] S. Devaraj, M. Kuezma, C. Ng, and P. Balaya, "Sol–gel derived nanostructured Li2MnSiO4/C cathode with high storage capacity," *Electrochimica Acta*, vol. 102, pp. 290–298, 2013.

[28] T. Boyadzhieva, V. Koleva, P. Markov, and R. Stoyanova, "Iron oxidation to amplify the Na and Li storage capacities of nano-sized maricite NaFePO4," *Dalton Transactions*, vol. 50, no. 45, pp. 16548–16561, 2021.

[29] C. Y. Chen, K. Matsumoto, T. Nohira, C. Ding, T. Yamamoto, and R. Hagiwara, "Charge–discharge behavior of a Na2FeP2O7 positive electrode in an ionic liquid electrolyte between 253 and 363 K," *Electrochimica Acta*, vol. 133, pp. 583–588, 2014.